Zeitschrift für Kristallographie 155, 27–45 (1981)

Structure refinements of seven natural olivine crystals and the influence of the oxygen partial pressure on the cation distribution

G. Nover and G. Will

Mineralogisches Institut, Lehrstuhl für Mineralogie und Kristallographie
der Universität Bonn, Poppelsdorfer Schloß, D-5300 Bonn 1, Federal Republic of Germany

Received: February 21, 1980

Abstract. Mg/Fe order in olivine has been determined by X-ray diffraction data, for example by Wenk and Raymond (1973). We have now studied the dependence of the Mg/Fe order vs. oxygen partial pressure. Two natural olivine samples of volcanic origin containing respectively 10 and 12 % fayalite were selected. The atomic positions, anisotropic temperature factors, extinction coefficient and site occupancies have been refined to R-values of 2.2 %. In total seven crystals were studied and the distribution coefficients K_D determined. A significant change in the Mg/Fe order could be detected after subjecting five of the crystals to well defined oxygen partial pressure conditions of 10^{-16} and 10^{-21} bar. An increase of K_D from 1.09 and 1.06 (natural) to 1.20 under low pO_2 conditions could be observed. This means higher order for Fe in $M1$. A decrease to $K_D = 0.80$ was found under high pO_2 conditions, meaning higher order for Fe in $M2$.

These experiments seem to indicate that the prevailing oxygen partial pressure determines the different Mg/Fe order found in natural olivine crystals.

1. Introduction

The basic structure of olivines (Bragg and Brown, 1926) is a close packing of oxygen with Mg and Fe occupying one half of the distorted octahedral interstices, known as $M1$ and $M2$ sites, and Si occupying one-eights of the tetrahedral interstices (Fig. 1). Several structures of olivines of different compositions have been refined from X-ray data with emphasis on structural variations. In recent years this interest has been concentrated on the determination of the Mg/Fe solid solution series. Earlier work on isostructural compounds like monticellite $CaMgSiO_4$ (Onken, 1965) and glauchroite $CaMnSiO_4$ (Caron et al., 1965) has shown that the cations are ordered in

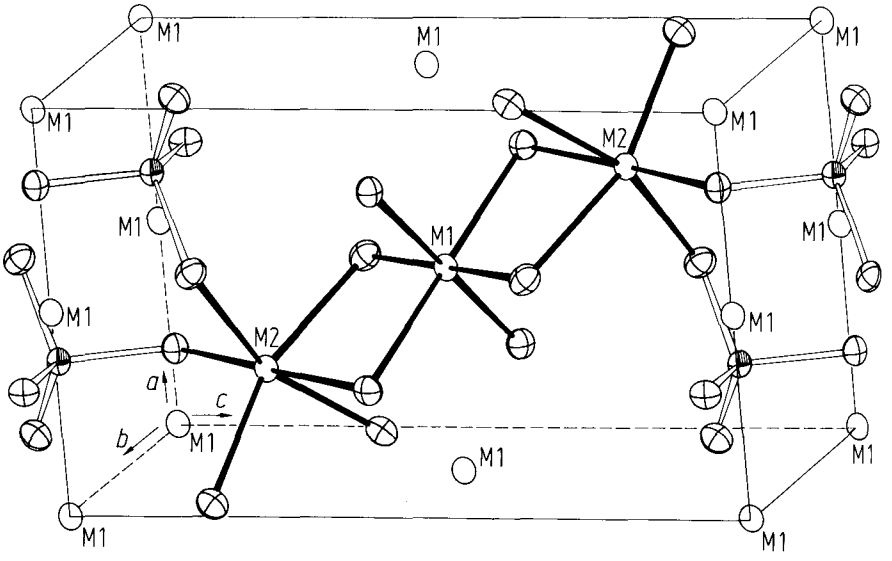

Fig. 1. An ORTEP drawing of the crystal structure of olivine

these crystals and this has stimulated researchers to look for ordering also in olivines.

For the Fe–Mn- and Mg–Mn-olivines (Brown, 1970; Huggins, 1973) and Ni–Mg-olivines (Rajamani, Brown and Prewitt, 1975) cation ordering derived from X-ray diffraction is in agreement with cation distributions predicted by Burns (1970). For the Mg–Fe olivines however the problem of cation ordering in the two distinct octahedral sites $M1$ (point symmetry C_i-$\bar{1}$) and $M2$ (point symmetry C_s-m) has become a controversial subject in the last years.

Partial order was first derived from spectroscopic measurements (Burns, 1970; Bush et al., 1970) but the results were not conclusive (Burns, 1970). The latest development of X-ray single crystal diffractometers has greatly improved the quality of the measured X-ray data and thus improved the resolution of such crystal structure refinements. It is possible today to determine electron densities in fraction of an electron. The Mg/Fe distribution and the cation ordering has been measured in several Mg–Fe olivines and in these investigations different degrees of ordering were detected in different crystals. It was not possible, however, to find a correlation between the ordering parameter and thermodynamic parameters, like for example the temperature. For the purpose of describing the cation ordering over the positions $M1$ and $M2$ we define a distribution coefficient

$$K_D = \frac{\mathrm{Mg2} \cdot \mathrm{Fe1}}{\mathrm{Mg1} \cdot \mathrm{Fe2}}. \tag{1}$$

Mg2 stands for Mg on $M2$ etc. K_D is related to the exchange reaction

$$\text{Fe}(M2) + \text{Mg}(M1) \rightleftharpoons \text{Fe}(M1) + \text{Mg}(M2). \quad (2)$$

Finger (1970) and Finger and Virgo (1971) studied a volcanic olivine crystal from Australia, and a lunar olivine crystal from rock 10020, both of which are believed to have rapid cooling histories. Both samples were reported to show a preference of Fe for the smaller $M1$ site (see also the data points in Fig. 5). In contrast Wenk and Raymond (1973) in a similar study report a preference of Fe for $M2$ in a metamorphic crystal with about 9 mol% fayalite. Brown (1973), in another study describes small order, which he thinks is insignificant. In his high temperature experiments he finds an increasing distortion of the $M1$ site with increasing temperature. Using electron spin resonance techniques Chatlein and Weeks (1973) have found Fe^{3+} exclusively at the $M1$ position, on the other hand Zeira and Hafner (1973) found statistical distribution of Fe^{3+} between the $M1$ and $M2$ sites.

The results accumulated so far, do not lead to an unambiguous picture for Mg/Fe ordering in olivines and no underlying principle has been proposed to explain the results. Obviously there is no convincing correlation of K_D, the distribution coefficient, to the composition; and the quite differnt cooling histories of the crystals tend to have only minor influence on the Mg–Fe ordering.

From measurements of the electrical conductivity of olivines (Will, Cemic, Hinze, Seifert and Voigt, 1979) we have found that the prevailing oxygen partial pressure is influencing greatly the physical properties of these crystals. We have therefore started to explore also the influence of the oxygen partial pressure on the crystal structure of olivines, especially on the cation ordering. This parameter has up to now been neglected. It is our suggestion that the oxygen partial pressure is the significant driving force for the cation ordering on the $M1/M2$ sites in olivines, and we believe we can demonstrate a correlation between the cation distribution and the prevailing oxygen partial pressure.

Our interest has been concentrated on olivines of volcanic origin and we have chosen for our studies natural crystals from the Dreiser Weiher, a quarternary Maar-volcano of the West Eifel, Federal Republic of Germany. In this locality olivines of different compositions are found in ultramafitic nodules, which have reliable analytical data and indications about the cooling histories available (Frechen, 1963; Vieten, 1973).

In this paper we wish to report the results of several refinements of the structures of differently treated crystals taken from two olivine samples collected at the Dreiser Weiher. The samples are labelled *FE*10 and *FE*12 referring to their fayalite content of 10 mol% Fa and 12 mol% Fa respectively. The results of wet chemical and microprobe analysis are listed in Table 1. From this analysis we calculate the actual compositions of

Table 1. Analytical data (weight %) of the two olivine samples *FE* 10 and *FE* 12

	FE 10	*FE* 12	Mol %	*FE* 10	*FE* 12
SiO_2	39.48	40.29	Mg_2SiO_4	88.50	86.00
MgO	48.70	46.62	Fe_2SiO_4	10.72	12.60
FeO	10.51	12.18			
Fe_2O_3	0.14	0.69			
NiO	0.31	0.28			
CaO	0.33	0.34			
Al_2O_3	n. d.	0.05			
H_2O^+	0.40	n. d.			
H_2O^-	0.15	n. d.			
	100.02	100.45		99.22	98.60

$Al_2O_3 < 0.005$

$Mg_{1.771}Fe_{0.214}Ni_{0.006}Ca_{0.009}(SiO_4)$ and $Mg_{1.724}Fe_{0.260}Ni_{0.006}Ca_{0.009}(SiO_4)$. We first studied the Mg/Fe distribution over *M* 1 and *M* 2 in the natural untreated crystals. Then we subjected the crystals to various, well defined oxygen partial pressures and studied afterwards the crystals again by X-ray diffraction, thus determining the influence of the oxygen fugacity on the cation distribution.

2. Experimental procedures

a) Crystal selection

Small crystals ranging in size from 0.5 to 4.0 mm were seperated from the nodules. From about two hundred crystals of *FE* 10 and eighty crystals of *FE* 12 only about 20 crystals were found to be free of twinning, intergrowth or cracks by examination under a polarization microscope. For the ensuing measurements on the four-circle-diffractometer these crystals were ground to spheres of about 0.2 mm diameter, a process which tends to introduce cracks. Finally 10 crystals *FE* 10 and 5 crystals *FE* 12 were available for X-ray investigations.

b) Data collection

The measurements were done on a computer controlled four-circle-diffractometer (Syntex $P2_1$) with Mo$K\alpha$ radiation ($\lambda = 0.71069$ Å) and a graphite monochromator ($2\theta = 12.2°$). The unit cell parameters were determined by least squares calculations from the adjusted settings of 25 independent reflexions. The intensity data were collected in the $\theta - 2\theta$ scan mode with a 1.0° plus (α_1, α_2) dispersion scan range. The maximum value of 2θ was 80° ($\sin\theta/\lambda = 0.9$ Å^{-1}). The scan speed was adjustable between 0.5

Table 2. Summary of crystal data and data collection

Wave length:	$\lambda = 0.71069$ Å; $2\theta_{max} = 80°$ ($\sin\theta/\lambda = 0.9$ Å^{-1})						
Space group:	*Pnma*						
Crystal size diameter:	0.19–0.21 mm						
	*FE*10 natural	*FE*10 *PU*	*FE*10 *P*1	*FE*12 natural	*FE*12 *P*2	*FE*12 *P*3	*FE*12 *P*4
μ(Mo$K\alpha$)	20 cm^{-1}			22 cm^{-1}			
Number of refl. incl. stand.	2483	2610	1578	2256	1976	2259	2499
Unique refl.	976	978	979	980	975	975	975
Unobs. ($I < 2.5\sigma$)	164	110	138	120	59	59	36

Table 3. Lattice constants of the olivine crystals before (a) and after buffering (b), estimated standard deviations in parenthesis

		a_0	b_0	c_0
*FE*10	(a)	6.0027(9)	4.7673(7)	10.2391(10)
*FE*10 *PU*	(b)	6.0028(8)	4.7673(6)	10.2424(8)
*FE*10 *P*1	(b)	6.0030(6)	4.7679(5)	10.2448(6)
*FE*12	(a)	6.005(1)	4.7687(8)	10.2773(11)
*FE*12 *P*2	(b)	6.004(1)	4.7678(6)	10.2729(10)
*FE*12 *P*3	(b)	6.004(1)	4.7674(4)	10.2719(10)
*FE*12 *P*4	(b)	6.004(1)	4.7676(8)	10.2731(15)

and 14.65° per minute and the total background counting time equalled the time spent for the peak count. Four standard reflexions 211, $\overline{2}11$, 113, $\overline{1}13$ were measured after every 30 reflexions. In the data reduction the intensities were adjusted to the fluctuations of the sums of the standards. Measurements were performed in the *hkl* and *hkl̄* octants, related reflexions were averaged resulting in a set of 980 unique reflexions for each crystal. Reflexions with $I < 2.5\sigma$ were considered unobserved. No absorption correction was applied ($A = 1.80$ for $2\theta = 0°$ and $A = 1.76$ for $2\theta = 80°$ in the case of *FE*10). The results of the crystal measurements and data collection are summarized in Table 2. Table 3 lists the lattice parameters of all crystals investigated, including the values of the crystals after buffer treatment.

c) Structure refinement

Refinements of the structures were carried out using a local version of the full matrix least squares program ORFLS (Busing, Martin, and Levy, 1962)

extended for the refinement of the occupation numbers on $M1$ and $M2$. Atomic scattering factors were taken for Fe^{2+}, Mg^{2+}, Si^0, O^0 from Cromer and Mann (1968). Anomalous scattering was considered for Fe (Cromer, 1965). The reflexions were weighted with their own sigmas [$w = 1/\sigma^2(F)$] as well as with a Cruickshanck (1961) weighting scheme. All atoms were refined for anisotropic thermal vibration, secondary extinction were taken into account according to Zachariasen (1963).

The multiplicity factors in the least squares calculations scale the scattering factors and hence may serve to count the numbers of electrons assigned to each site effectively. From the multiplicity factors the occupation numbers can be calculated and from them the cation ordering.

A least squares refinement of site occupancies has to take into account constraints imposed by the chemical composition and the electroneutrality of the crystals. If we define a_{mn} as the fractional occupancy of the site m by the chemical species n, then the equation

$$\sum_n a_{mn} \leqslant 1 \tag{3}$$

must be satisfied as a first constraint. As a second constraint the site chemistry must agree with the bulk chemistry, known from the chemical analysis (Table 1). With c_n = the total number of atoms of the species n (Mg and Fe) per unit cell or per formula unit, and b_m the multiplicity of the site m we get

$$\sum_m b_m \cdot a_{mn} = c_n . \tag{4}$$

The formal solution of this problem has been derived by Raymond (1972). For the present case we can express these conditions by a matrix:

n \ m	$M1$	$M2$
Fe	a_{11}	a_{12}
Mg	a_{21}	a_{22}

c_1 and c_2 of Eq. (4) can be calculated from the chemical analysis. In the case of $FE10$ we get $c_1 = 0.216$ (concentration of Fe-ions per formula unit), and $c_2 = 1.784$ (concentration of Mg-ions per formula unit). In the least squares calculation it suffices to refine only one variable, $V_1 = a_{11}$ (=Fe on $M1$), while the other parameters are determined through the constraints C_1, C_2 and C_3. This is compactly expressed in matrix notation.

$$Q = \begin{bmatrix} 1 & 0 & 0 & 0 \\ b_1 & b_2 & 0 & 0 \\ b_1 & 0 & b_3 & 0 \\ b_1 & b_2\,\mathrm{Mg/Fe} & 0 & b_4\,\mathrm{Mg/Fe} \end{bmatrix} \cdot \begin{bmatrix} a_{11}\,(\mathrm{Fe}M1) \\ a_{12}\,(\mathrm{Mg}M1) \\ a_{21}\,(\mathrm{Fe}M2) \\ a_{22}\,(\mathrm{Mg}M2) \end{bmatrix} = \begin{bmatrix} V_1 \\ C_1 \\ C_2 \\ C_3 \end{bmatrix} \tag{5}$$

The first constraint C_1 imposes the full occupancy of $M1$. The second constraint C_2 introduces the chemistry through the total amount of Fe known from the chemical analysis, and the third constraint C_3 contains the total charge at the positions $M1$ and $M2$, which is calculated from the chemical composition. From the values a_{mn} which have been determined by least squares refinement procedure for all crystals, the distribution coefficient K_D can be calculated (Eq. 1).

3. Crystal structure refinements

In total we have made seven measurements and structure refinements on the two types of crystals *FE*10 and *FE*12. Two measurements were on the original natural crystals and five measurements on the crystals after being treated by different buffering processes. The buffering conditions are summarized in Table 4.

a) Buffer treatment

Since we expect that the Mg/Fe distribution should depend on the oxygen partial pressure, we have treated the crystals by two pO_2-pressures as defined by the two different buffer mixtures, namly *QFM*, consisting of quartz,

Table 4. Experimental data for the buffer treatments

Sample	pO_2 (bar)	T (°C)	h	Buffer	
*FE*10 → *FE*10*PU*	10^{-16}	750	25	$Fe_3O_4/SiO_2/Fe_2SiO_4$	*QFM*
(*FE*10) → *FE*10*P*1	10^{-21}	750	20	$Fe/SiO_2/Fe_2SiO_4$	*QFI*
*FE*12 → *FE*12*P*2 (*FE*12) → *FE*12*P*3	10^{-21}	750	66	$Fe/SiO_2/Fe_2SiO_4$	*QFI*
↓ *FE*12*P*4	10^{-16}	750	24	$Fe_3O_4/SiO_2/Fe_2SiO_4$	*QFM*

Table 5. Summary of R-values for all crystals studied

	*FE*10	*FE*10*P*1	*FE*10*PU*	*FE*12	*FE*12*P*2/3	*FE*12*P*4
R_{overall}	0.0304	0.0361	0.0389	0.0263	0.0328	0.0228
$R_{\text{omitting unobs.}}$	0.0208	0.0279	0.0337	0.0202	0.0300	0.0217
$R_{\text{weighted overall}}$	0.0306	0.0363	0.0392	0.0255	0.0321	0.0220
$R_{\text{weight.om. unobs.}}$	0.0198	0.0252	0.0331	0.0198	0.0274	0.0209

Table 6. Occupation numbers for Fe and Mg on the two sites ($M1$) and ($M2$), and distribution coefficient K_D

	($M1$)		($M2$)		K_D
	Fe	Mg	Fe	Mg	
*FE*10	0.1124(7)	0.8876	0.1036	0.8964	1.09(1)
*FE*10 *P*1	0.1168(10)	0.8832	0.0992	0.9008	1.20(2)
*FE*10 *PU*	0.0974(10)	0.9026	0.1186	0.8814	0.80(2)
*FE*12	0.1394(5)	0.8606	0.1336	0.8670	1.06(1)
*FE*12 *P*2/3	0.1464(10)	0.8526	0.1256	0.8744	1.20(2)
*FE*12 *P*4	0.1380(8)	0.8620	0.1340	0.8660	1.03(1)

fayalite and magnetite, and *QFI*, consisting of quartz, fayalite and iron (Will and Nover, 1979). At constant $T = 750$ °C we have a pO_2 pressure of 10^{-21} bar for *QFI* and of 10^{-16} bar for *QFM*. These values are determined by the buffer composition and the given temperature. After each buffer treatment the crystals were studied again as described by a complete X-ray diffraction analysis and their structures refined. The lattice constants of all crystals are included in Table 3, the corresponding R-values are given in Table 5 and the occupation numbers together with the occupation coefficients K_D in Table 6. The standard deviation of Fe$M1$ is given in parenthesis. The error of this value is about 0.4% for all crystals ($K_D = \pm 1.5\%$). Figure 1 depicts the K_D distribution coefficient of this paper together with previous measurements taken from literature.

b) Atomic positions and bond length

The atomic positions and temperature factors are listed in Tables 7 and 8 for all crystals of composition *FE*10 and *FE*12. Figure 2 depicts an ORTEP-drawing of the structural section containing $M1$ and $M2$ showing the coordination of these sites. From the atomic positions interatomic distances were calculated and selected values are given in Table 9. The mean $M1-O$, $M2-O$ and $Si-O$ distances are plotted in Figure 3 together with values reported in the literature. Within the same composition no differences in the bond length of the mean $M1-O$ and $M2-O$ distances are to be observed implying that there is no correlation between K_D and the bond length. The same observation holds for the bond angles, which are tabulated in Table 10.

c) Temperature factors

Anisotropic temperature factors were included in the refinement, and the results are included in Tables 8 and 9. We realize that the temperature factors

Table 7. Atomic coordinates for the seven olivines

		*FE*10	*FE*10 *P*1	*FE*10 *PU*	*FE*12	*FE*12 *P*2/3	*FE*12 *P*4
(*M*1)	*x*	0.0	0.0	0.0	0.0	0.0	0.0
	y	0.0	0.0	0.0	0.0	0.0	0.0
	z	0.0	0.0	0.0	0.0	0.0	0.0
(*M*2)	*x*	0.25	0.25	0.25	0.25	0.25	0.25
	y	−0.0103(1)	−0.0107(2)	−0.0102(2)	−0.0104(2)	−0.0105(2)	−0.0105(2)
	z	0.27773(6)	0.27773(9)	0.27776(9)	0.27782(8)	0.27782(8)	0.27779(6)
Si	*x*	0.25	0.25	0.25	0.25	0.25	0.25
	y	0.4267(1)	0.4268(1)	0.4268(1)	0.4270(1)	0.4268(1)	0.42688(9)
	z	0.09446(5)	0.09445(6)	0.09436(6)	0.09454(5)	0.09455(5)	0.09458(2)
O1	*x*	0.25	0.25	0.25	0.25	0.25	0.25
	y	0.7662(2)	0.7659(3)	0.7661(3)	0.7660(3)	0.7659(3)	0.7662(2)
	z	0.0917(1)	0.0916(1)	0.0920(2)	0.0918(1)	0.0917(1)	0.0916(1)
O2	*x*	0.25	0.25	0.25	0.25	0.25	0.25
	y	0.2208(2)	0.2206(3)	0.2203(3)	0.2203(3)	0.2205(3)	0.2199(2)
	z	0.4475(1)	0.4476(1)	0.4476(1)	0.4477(1)	0.4478(1)	0.4478(1)
O3	*x*	0.0336(1)	0.0333(2)	0.0333(2)	0.0334(1)	0.0332(2)	0.0335(1)
	y	0.2784(2)	0.2785(2)	0.2786(2)	0.2788(2)	0.2786(2)	0.2787(1)
	z	0.1634(1)	0.1634(1)	0.1634(1)	0.1634(1)	0.1633(1)	0.16333(7)

Table 8. Anisotropic temperature factors for the olivines ($\times 10^{-4}$)

		*FE*10	*FE*10 *P*1	*FE*10 *PU*	*FE*12	*FE*12 *P*2/3	*FE*12 *P*4
(*M*1)	β(1,1)	29(2)	31(2)	27(2)	26(1)	37(3)	25(1)
	(2,2)	37(2)	57(3)	43(3)	36(2)	54(3)	39(2)
	(3,3)	13.7(5)	11.0(6)	12.3(7)	12.3(5)	12.0(6)	12.6(4)
	(1,2)	3(1)	3(2)	4(2)	4(1)	3(2)	4(1)
	(1,3)	3.8(7)	3.7(9)	3.2(8)	4(1)	4(1)	4(1)
	(2,3)	1.3(1)	1.2(1)	1.3(1)	0.7(1)	1.0(1)	0.4(9)
(*M*2)	β(1,1)	33(2)	34(2)	38(2)	31(1)	37(3)	31(1)
	(2,2)	51(2)	69(3)	66(3)	54(3)	67(3)	57(2)
	(3,3)	9(4)	7(6)	7(7)	9.5(5)	7.9(5)	9.0(2)
(1,2)=(1,3)		0	0	0	0	0	0
	(2,3)	0.40(9)	0.1(1)	0.1(1)	0.70(9)	1.0(1)	1.0(1)
Si	β(1,1)	27.5(9)	31(1)	28(1)	23.9(9)	33(2)	23.3(8)
	(2,2)	26(1)	41(2)	37(2)	27(1)	43(2)	29(1)
	(3,3)	9(3)	7(4)	7(4)	7.9(3)	7.2(3)	8.4(2)
(1,2)=(1,3)		0	0	0	0	0	0
	(2,3)	0.2(9)	1(7)	0.4(7)	0.2(6)	0.7(6)	1.3(4)
O1	β(1,1)	41(3)	41(3)	22(3)	34(2)	43(5)	32(2)
	(2,2)	46(4)	48(5)	42(5)	33(4)	47(4)	36(3)
	(3,3)	10(1)	13(1)	20(1)	15.3(8)	13.8(9)	14.3(9)
(1,2)=(1,3)		0	0	0	0	0	0
	(2,3)	2(1)	2(2)	2(2)	0.1(1)	0.1(1)	0.1(1)
O2	β(1,1)	42(3)	42(3)	21(3)	38(2)	46(5)	36(2)
	(2,2)	46(4)	66(5)	60(5)	50(4)	60(5)	55(3)
	(3,3)	10(1)	7.5(9)	16(1)	9.3(8)	8.3(9)	9.6(6)
(1,2)=(1,3)		0	0	0	0	0	0
	(2,3)	2(1)	1(2)	1(2)	1(1)	1(1)	1(1)
O3	β(1,1)	37(2)	37(2)	19(2)	37(2)	40(4)	33(1)
	(2,2)	46(3)	69(3)	59(3)	49(3)	64(3)	51(2)
	(3,3)	14(5)	13(5)	19(6)	13.9(5)	12.7(6)	13.5(4)
	(1,2)	− 3(2)	− 1(2)	− 3(2)	− 2(2)	− 2(2)	− 2(1)
	(1,3)	5.1(8)	5(1)	5(1)	4.4(8)	3.0(1)	4.8(7)
	(2,3)	0.6(9)	7(1)	3(1)	0.2(1)	0.1(1)	0.2(1)

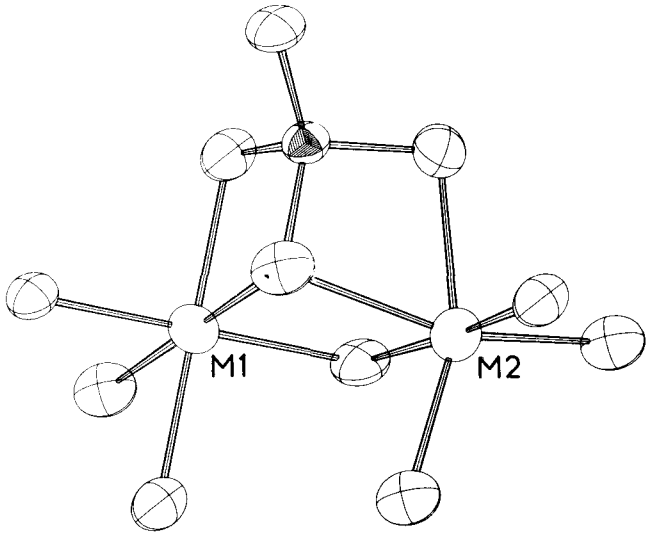

Fig. 2. An ORTEP drawing of a section of the structure of olivine around *M* 1 and *M* 2 showing the tetrahedral and octahedral coordination of Si and of the cations resp.

for the buffered crystals are larger than those for the original natural crystals *FE* 10 and *FE* 12. Since a change in K_D means an exchange of Mg and Fe between the sites *M* 1 and *M* 2 this process may well introduce structural defects and therefore higher vibrational coefficients. Figure 2 allows one to see this anisotropy of the polyeder *M* 1, *M* 2 and Si with the surrounding oxygen atoms.

d) Extinction

Some strong low angle reflexions showed large discrepancies in the first stages of the refinement. A correction for isotropic secondary extinction was therefore included in the refinement according to Zachariasen (1968). The results are included in Tables 7 and 8. The buffered crystals have larger *g*-values than the natural untreated crystals, indicating that the process of buffering introduces structural defects, which is not surprising.

e) Charge density

Wenk and Raymond (1973) have calculated approximated formal electrical charges for each atom from the refined scale factors. Such results cannot be conclusive and accordingly their calculations did not converge. The proper

Table 9. Selected interatomic distances

	*FE*10	*FE*10 *P*1	*FE*10 *PU*	*FE*12	*FE*12 *P*2/3	*FE*12 *P*4
(1) Si–O(1)	1.619(1)	1.618(2)	1.618(2)	1.616(2)	1.616(2)	1.618(1)
(1) Si–O(2)	1.661(1)	1.661(2)	1.658(2)	1.660(2)	1.659(2)	1.662(1)
(2) Si–O(3)	1.639(1)	1.640(1)	1.641(1)	1.640(2)	1.639(1)	1.639(1)
⟨Si–O⟩	1.639(1)	1.639(2)	1.639(2)	1.639(2)	1.638(2)	1.639(1)
(2) *M*1–O(1)	2.092(1)	2.093(1)	2.094(1)	2.094(2)	2.092(1)	2.093(1)
(2) *M*1–O(2)	2.077(1)	2.078(1)	2.078(1)	2.079(2)	2.076(1)	2.079(1)
(2) *M*1–O(3)	2.145(1)	2.147(1)	2.146(1)	2.147(1)	2.145(1)	2.150(1)
⟨*M*1–O⟩	2.105(1)	2.106(1)	2.106(1)	2.107(2)	2.104(1)	2.107(1)
(1) *M*2–O(1)	2.183(2)	2.185(2)	2.181(2)	2.184(2)	2.184(2)	2.189(1)
(1) *M*2–O(2)	2.058(2)	2.060(2)	2.058(2)	2.059(2)	2.060(2)	2.064(1)
(2) *M*2–O(3)	2.068(1)	2.066(1)	2.066(1)	2.066(2)	2.066(1)	2.067(1)
(2) *M*2–O(3′)	2.226(1)	2.229(2)	2.226(1)	2.229(2)	2.228(1)	2.230(1)
⟨*M*2–O⟩	2.138(2)	2.139(2)	2.137(2)	2.139(2)	2.138(1)	2.141(1)

Table 10. Selected bond angles

		*FE*10	*FE*10 *PU*	*FE*10 *P*1	*FE*12	*FE*13 *P*2/3	*FE*12 *P*4
1	O(1)–Si–O(2)	114.03(9)	114.09(9)	114.01(9)	114.05(8)	113.98(9)	113.85(6)
2	O(1)–Si–O(3)	116.05(5)	115.93(6)	116.03(6)	116.00(5)	116.00(5)	116.03(4)
2	O(2)–Si–O(3′)	101.97(6)	102.03(7)	101.98(6)	101.98(5)	101.96(6)	102.07(4)
1	O(3)–Si–O(3′)	104.87(7)	104.97(8)	104.93(7)	104.96(6)	105.06(7)	104.92(5)
	⟨O–Si–O⟩	109.16(5)	109.16(7)	109.19(7)	109.16(8)	109.16(6)	109.16(4)
2	O(1)–*M*1–O(3)	84.97(5)	84.99(6)	85.05(6)	84.98(5)	85.01(5)	84.90(4)
2	O(1)–*M*1–O(3′)	95.03(5)	95.01(6)	94.95(6)	95.02(5)	94.99(5)	95.10(4)
2	O(1)–*M*1–O(2′)	93.48(5)	93.43(5)	93.43(5)	93.44(4)	93.51(4)	93.44(3)
2	O(1′)–*M*1–O(2′)	86.52(5)	86.57(5)	86.57(5)	86.56(4)	86.49(4)	86.56(3)
2	O(2)–*M*1–O(3′)	105.23(5)	105.24(5)	105.24(5)	105.30(5)	105.27(5)	105.28(4)
2	O(2)–*M*1–O(3)	74.77(5)	74.76(6)	74.76(5)	74.70(5)	74.73(5)	74.72(4)
	⟨O–*M*1–O⟩	90.00(5)	90.00(6)	90.00(6)	90.00(5)	90.00(5)	90.00(4)
2	O(1)–*M*2–O(3″)	90.95(5)	90.90(5)	90.99(5)	90.96(5)	91.02(5)	91.10(3)
2	O(1)–*M*2–O(3′)	80.95(5)	81.06(6)	80.97(5)	80.97(5)	80.90(5)	80.80(4)
2	O(2)–*M*2–O(3″)	90.84(5)	90.80(5)	90.80(5)	90.78(5)	90.75(5)	90.64(3)
2	O(2)–*M*2–O(3′)	96.50(6)	96.55(5)	96.48(6)	96.56(5)	96.58(6)	96.73(4)
1	O(3′)–*M*2–O(3″)	71.43(5)	71.55(5)	71.41(5)	71.39(5)	71.45(5)	71.30(4)
2	O(3′)–*M*2–O(3)	88.50(4)	88.48(5)	88.53(4)	88.49(4)	88.49(5)	88.56(3)
1	O(3′)–*M*2–O(3)	110.84(6)	110.76(6)	110.82(6)	110.91(6)	110.86(6)	110.87(4)
	⟨O–*M*2–O⟩	89.89(4)	89.84(5)	89.81(5)	89.82(6)	89.82(5)	89.82(4)

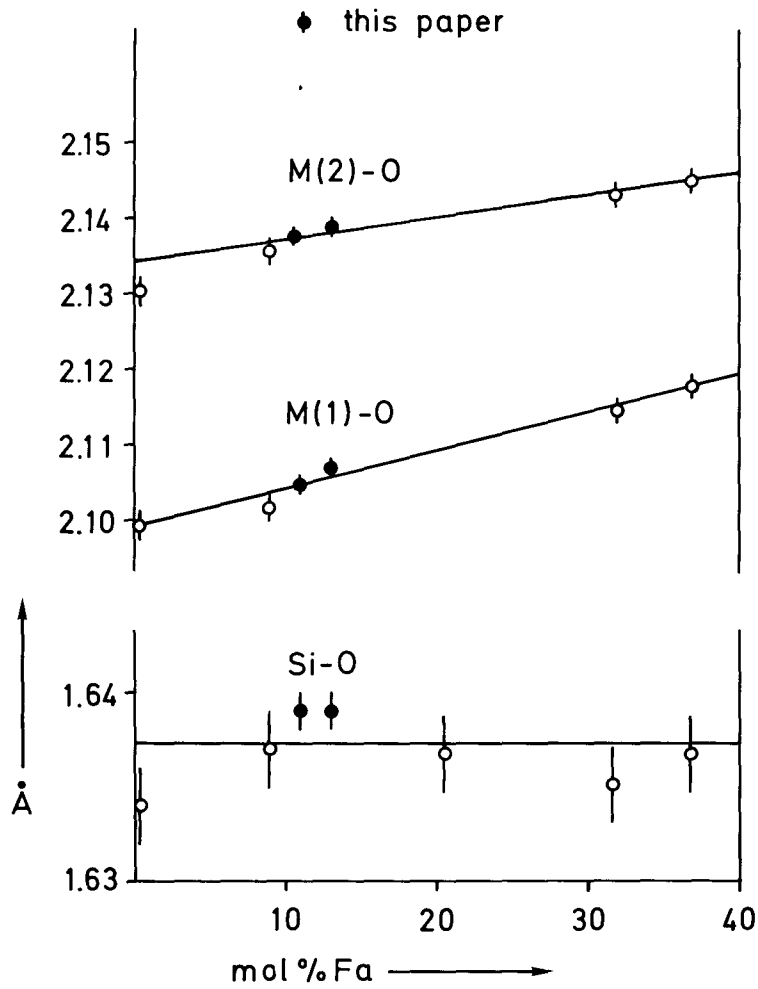

Fig. 3. The mean $M1-O$, $M2-O$ and $Si-O$ distances as a function of the fayalite content for several olivines, including selected results from the literature

way to calculate the formal charge of the SiO_4 tetrahedra is by interpretation of the electron densities from difference Fourier maps as shown in Figure 4. We have studied recently bonding features and point charges in the $[S_2O_6]^{2-}$ complex of $Na_2S_2O_6 \cdot 2H_2O$ (Kirfel, Will, and Weiss, 1979) and in the $[SO_4]^{2-}$ tetrahedron of $CaSO_4$ (Kirfel and Will, 1980) and we have applied this method also to the $[SiO_4]^{4-}$ tetrahedron. Different structural models based on the refined multiplicity factors for Si and oxygen were selected and

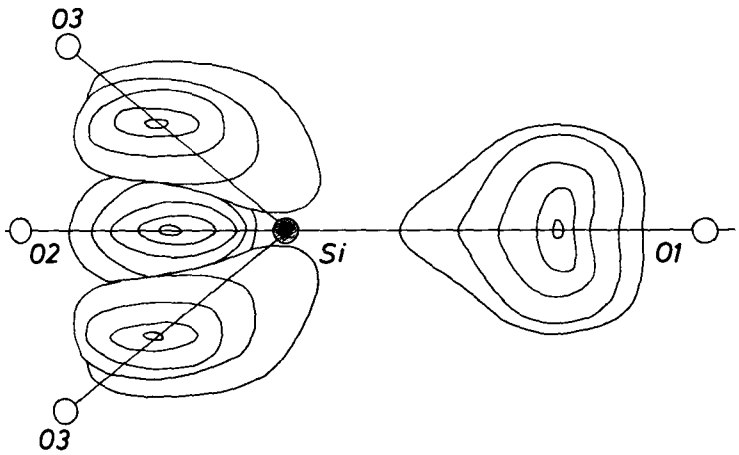

Fig. 4. Electron density distribution from difference Fourier maps on the connections Si–O in the SiO_4 tetrahedra. Only the positive contours are drawn at intervals of 0.025 el/Å^3

in addition we included point charges ($f = 1.0$) on the Si–O bonds in the refinement. These calculations verify the picture of the four fold negative SiO_4-tetrahedron with covalent charge distributions on the Si–O bonds leading to $Si^{+0.5}$ for the silicon atoms, to $O^{-0.52}$ for the oxygen atoms and to covalent charges of 0.6 electrons on the Si–O bonds. Further experiments are now under way to calculate difference Fourier maps also in other sections in order to establish precisely the charge and valence distributions in the $[SiO_4]^{4-}$ tetrahedron and around the $M1$ and $M2$ sites.

4. Discussion

In recent years several authors have investigated the possibility to use the Mg–Fe distribution as a means of obtaining information on the temperature of crystallization and also on the equilibrium cooling history of minerals. In the case of pyroxenes and amphiboles (Ghose and Weidner, 1972; Seifert and Virgo, 1974, 1975; Virgo and Hafener, 1969), such investigations revealed a correlation between the cation distribution and the genesis of the crystals. Decreasing temperatures induce a migration of Fe^{2+} from positions with small volumes to others with greater volumes. The cation distribution is thereby influenced by factors such as coordinating ligands, charge balance considerations, polyhedron distortion, electronegativity, or polarizability of the cation and ionic radii involved (Bancroft and Burns, 1967; Burns, 1970;

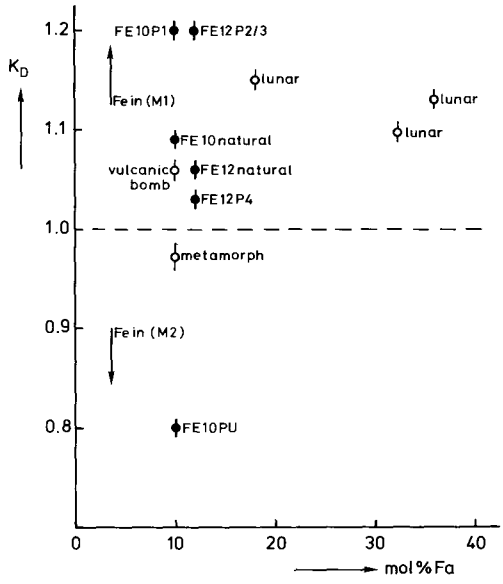

Fig. 5. The distribution coefficient K_D vs. mol % fayalite as determined from the X-ray diffraction refinements presented in this paper (●). Included in the diagram are values from the literature (○)

Fisher, 1966; Finger, 1969). This result is in agreement also with Parthé's observation (Parthé, 1969) of anion packing, where the filling of vacant sites should mainly depend on the ionic radii of the inserted cations. In addition, Burns (1970) showed that Fe^{2+} is most stable when it occupies the most distorted site.

This picture works well in explaining the cation distributions in pyroxenes and amphiboles, but it fails in the case of olivine crystals. Here the exchange takes place between two octahedral coordinated sites of only slightly different volume ($M1/M2 = 0.95$) and no correlation could be found between the measured Mg/Fe cation distributions and temperature conditions or/and genetical conditions (Burns, 1970; Bush, Hafner, and Virgo, 1970; Finger and Virgo, 1971; Smyth and Hazen, 1973).

Burns (1970) concluded from metamorphic olivines that the cation radii might be responsible for the detected order, and gave an explanation with crystal field theory. When further investigations on volcanic and lunar olivine crystals showed just the opposite behaviour the size argument had to be given up and temperature was considered of importance for the cation distribution. But high temperature experiments did not lead to a significant change of the ordering in olivine crystals (Virgo and Hafner, 1972; Smyth and Hazen, 1973).

On the other hand it was realized from measurements of electrical conductivities on olivines and pyroxenes by Will et al. (1979), that the prevailing oxygen fugacity strongly influences the physical properties of these crystals.

With this in mind we checked some olivine crystals for their petrological history. Different pO_2 conditions during crystallization were assumed by Frechen (1963) and Vieten (1973) from their fairly well known petrological past. The influence of the oxygen fugacity on the K_D could then be confirmed by X-ray investigations (Will and Nover, 1979). Higher iron concentration on $M1$ ($K_D > 1$) is correlated with a decrease of pO_2. This result could be further substantiated experimentally by exposing these crystals to low (10^{-21} bar) and high (10^{-16} bar) oxygen partial pressure conditions (Will and Nover, 1979). Treating the same crystal twice, first with low and then with high pO_2 conditions led to a significant change of the K_D value. At the same time also a dependence of the equilibrium cation distribution on the exposure time could be detected. The results accumulate so far tend to show a nearly linear dependence of K_D vs. pO_2, and this allows also an interpretation of previous results of other authors. The experiments reported in this paper seem to indicate that the cation distribution in olivine crystals is determined by the prevailing oxygen partial pressure and can be influenced by applying externally different pO_2 conditions.

Further experiments are now under way to calculate difference Fourier maps in order to establish precisely the charge and valence distributions around the $M1$ and $M2$ sites. Such calculations will also make sure, that there is no migration of Mg or Fe out of the crystal or into vacant octahederal lattice positions by the buffer treatment. With the limit of detectable electron difference densities of about 0.05 el/Å^3 it should be possible to detect such migrations. The calculations are done by scaling the electron densities at the positions $M1$ and $M2$ to the density of the unaffected SiO_4 tetrahedra as an internal standard. The first calculations performed for all crystals gave no loss of Mg and Fe during buffer treatment, e.g. all Mg and Fe could be found again in $M1$ and $M2$ after buffering.

The increase of the electrical conductivity under different pO_2 conditions is produced by an increase of the Fe^{3+} concentrations in these crystals (Duba, Heard, and Schock, 1974; Will et al., 1979). The concentration of Fe^{3+} in all crystals was beyond the experimental limit and these findings indicate that the chosen thermodynamic parameters gave no reason for detectable higher Fe^{3+} concentrations. In addition we have checked the Fe^{3+} concentration by Mößbauer measurements, kindly performed by Professor Hafner and Dr. Amthauer, Marburg, leading to less than $[y = 2 \times 10^{-5}/\text{mol} = (Fe_{Fe})/4]Fe^{3+}$ concentrations at 800° C.

Acknowledgement. We wish to thank Professor Frechen, Bonn, for providing the samples and for helpful discussions, as well as Drs. Hinze and Kirfel for many valuable discussions. Financial support by the Deutsche Forschungsgemeinschaft is gratefully acknowledged.

References

Bragg, W. L., Brown, G. B.: Die Struktur des Olivins. Z. Kristallogr. **63**, 538–556 (1926)

Brown, G. E.: Crystal Chemisty of the Olivines. Ph. D. Dissertation Virginia Polytechnic Institute and State University, Blacksburg Virginia, pp. 122 (1970)

Brown, G. E., Prewitt, C. T.: High Temperature Crystal Chemistry of Hortonolite. Am. Mineral. **58**, 577–587 (1973)

Buening, D. K., Buseck, P. R.: Fe–Mg Lattice Diffusion in Olivine. J. Geophys. Res. **78**, 6852–6862 (1973)

Burns, R. G.: Crystal Field Spectra and Evidence of Cation Ordering in Olivine Minerals. Am. Mineral. **55**, 1609–1632 (1970)

Burns, R. G.: Site preference of transiton metal ions in silicate crystal structures. Chem. Geol. Netherl. **17**, 275–283 (1970)

Bush, W. R., Hafner, S. S., Virgo, D.: Some Ordering of Iron and Magnesium at the Octahedrally Coordinated Site in a Magnesium rich Olivine. Nature **227**, 1339–1341 (1970)

Busing, W. R., Martin, K. O., Levy, H. A.: ORFLS, a FORTRAN crystallographic least squares program. ORNL-TM-305 1962

Caron, L. G., Santore, R. P., Newnham, R. E.: Magnetic Structure of $CaMnSiO_4$. J. Phys. Chem. Solids **26**, 927–930 (1965)

Chatlein, A., Weeks, R. A.: Electron Paramagnetic Resonance of Fe^{3+} in Forsterite (Mg_2SiO_4). J. Chem. Phys. **58**, 3722–3726 (1973)

Cromer, D. T.: Anomalous Dispersion Corrections Computed from Self Consistent Field Relativistic Dirac-Slater Wave Functions. Acta Crystallogr. **18**, 17–23 (1965)

Cromer, D. T., Mann, J. B.: X-ray Scattering Factors Computed from Numerical Hartree-Fock Wave Functions. Acta Crystallogr. **A 24**, 321–324 (1968)

Finger, L. W.: Fe/Mg Ordering in Olivines. Carn. Inst. year Book **69**, 302–305 (1971)

Finger, L. W., Virgo, D.: Confirmation of Fe/Mg Ordering in Olivines. Carn. Inst. Year Book **70**, 221–225 (1971)

Frechen, J.: Kristallisation, Mineralbestand, Mineralchemismus und Förderfolge der Mafite vom Dreiser Weiher in der Eifel. N. Jb. Min. Monatshefte 205–225 (1963)

Huggins, F. E.: Cation order in olivines: Evidence from vibrational spectra. Chem. Geol. **11**, 99–109 (1973)

Kirfel, A., Will, G., Weiss: submitted to Acta Crystallogr. 1979

Kirfel, A., Will, G.: submitted to Acta Crystallogr. 1980

Onken, H.: Die Verfeinerung der Kristallstruktur von Monticellit. Tschermaks Min. Pet. Mitt. **10**, 34–44 (1965)

Rajamani, V., Brown, G. E., Prewitt, C. T.: Cation Ordering in Ni–Mg Olivine. Am. Mineral. **60**, 292–299 (1975)

Raymond, K. N.: Application of Constraints to Derivates in Least Squares Refinement. Acta Crystallogr. **A 28**, 163–166 (1972)

Vieten, K.: Die kristallchemische Entwicklung der Klinopyroxene in den Vulkaniten des Siebengebirges. Habilitationsschrift Universität Bonn, Federal Republic of Germany 1973

Wenk, H. R., Raymond, K. N.: Four new structure refinements of olivine. Z. Kristallogr. **137**, 86–105 (1973)

Will, G., Cemic, L., Hinze, E., Seifert, K. F., Voigt, R.: Electrical Conductivity Measurements on Olivines and Pyroxenes Under defined Thermodynamic Activities as a Function of Temperature and Pressure. Phys. Chem. Minerals **4**, 189–197 (1979)

Will, G. Nover, G.: Influence of Oxygen Partial Pressure on the Mg/Fe Distribution in Olivines. Phys. Chem. Minerals **4**, 199–208 (1979)

Zachariasen, W. H.: The secondary extinction correction. Acta Crystallogr. **16**, 1139–1144 (1963)

Zeira, S., Hafner, S. S.: The Location of Fe^{3+} Ions in Forsterite (Mg_2SiO_4). Earth Planet. Sci. Lett. **21**, 201–208 (1973)

Cruickshank, D. W. J., Pilling, D. E., Bujosa, A., Lovell, F. M., Truter, M. R.: Computing methods and the phase problem in X-ray analysis. Oxford: Pergamon (1961)

Bancroft, G. M., Burns, R. G., Howie, R. A.: Determination of the cation distribution in the orthopyroxenes series by the Mößbauer effect. Nature **213**, 1221–1223 (1967)

Fisher, K. F.: A further refinement of the crystal structure of cummingtonite. Am. Min. **51**, 814–816 (1966)

Duba, A., Heard, H. C., Schock, R. N.: Electrical conductivity of olivine at high pressure and under controlled oxygen fugacity. J. Geophys. Res. **79**, 1667–1673 (1974)

Ghose, S., Weidner, J. R.: Mg^{2+}-Fe^{2+} order-disorder in cummingtonite, $(Mg,Fe)_7Si_8O_{22}(OH)_2$: A new geothermometer. Earth Planet. Sci. Lett. **16**, 346–354 (1972)

Seifert, F., Virgo, D.: Temperature dependence of intracrystalline Fe^{2+}, Mg distribution in a lunar anthophyllite. Carnegie Inst. Year Book **73**, 405–411 (1974)

Seifert, F., Virgo, D.: Kinetics of the Fe^{2+}–Mg, order disorder reaction in anthophyllites: Quantitative cooling rates. Science **188**, 1107–1109 (1975)

Smyth, J. R., Hazen, R. M.: The crystal structures of forsterite and hortonolite at several temperatures up to 900° C. Am. Min. **58**, 588–593 (1973)

Virgo, D., Hafner, S. S.: Temperature dependent Mg,Fe distribution in a lunar olivine. Earth Planet. Sci. Lett. **14**, 305–312 (1972)

Will, G., Nover, G.: X-Ray structure determination of the Mg/Fe distribution in natural olivines in dependence of the oxygen partial pressure. Phys. Chem. Minerals **3**, 95 (1978)